Applied Nanoscience (2022) 12:1859–1868
https://doi.org/10.1007/s13204-022-02462-1

ORIGINAL ARTICLE

Corrosion processes of silver nanoparticles

Vicki J. Keast[1]

Received: 2 December 2021 / Accepted: 2 March 2022 / Published online: 17 March 2022

Abstract
The corrosion of silver nanoparticles (AgNPs) on exposure to ambient air was studied using imaging and analysis in the scanning transmission electron microscope (STEM). Secondary particles are formed on exposure to ambient air, and these are more numerous and more widely distributed as the relative humidity increases. Energy-dispersive X-ray analysis (EDS) confirms that the particles contain Ag and S. Electron energy loss spectra (EELS) in the valence part of the spectrum (< ~ 50 eV) identify the corrosion product as Ag_2S on comparison with spectra from reference compounds. The EELS measurements also allow for a direct visualisation of the shift in the energy of the surface plasmon peak that occurs when the corrosion product is in contact with the particle. The experiments confirm that advanced electron microscopy methods have an important role in investigating corrosion of nanoparticulate systems.

Keywords Nanoparticle · Plasmonics · Corrosion · Silver · Silver Sulfide · Electron Energy Loss Spectroscopy

Introduction

Ag nanoparticles (AgNPs) are of significant technological interest for two quite distinct purposes: as an antibacterial (Alexander 2009; Barillo and Marx 2014); and for plasmonics (Rycenga et al. 2011). AgNPs are also notable for undergoing rapid corrosion in ambient air which places constraints on the applications for which they are suitable (Elechiguerra et al. 2005; McMahon et al. 2005; Keast et al. 2016). Ag has been identified as the ideal material for plasmonics applications as it can sustain very strong plasmon resonances (Pastoriza-Santos and Liz-Marzan 2008; Rycenga et al. 2011). However, it has failed to capitalise on this promise in many plasmonic applications due to its very rapid corrosion and, consequently, Au remains the material of choice, despite being less suitable and more expensive. Furthermore, the release of Ag^+ ions from AgNPs is an intrinsic aspect of both their antibacterial activity (Rizzello and Pompa 2014; Le Ouay and Sellacci 2015) and the mechanism by which the chemical transformations during corrosion occur (Gorham et al. 2014; Yu et al. 2014). Therefore, investigations into the corrosion processes can assist in understanding the antibacterial activity. In addition, in some medical applications, corrosion of the AgNPs before their use may impact their antibacterial effectiveness.

In the case of bulk Ag, corrosion occurs by reaction with trace amounts of H_2S and/or OCS in the atmosphere to produce Ag_2S (Franey et al. 1985). The corrosion product forms as a discontinuous layer of spherical particles and the particles increase in size but not density over time (Bennett et al. 1969). The rate of corrosion to Ag_2S is dependent on the presence of water vapour (Pope et al. 1968; Bennett et al. 1969; Graedel et al. 1985) and it is believed that the role of relative humidity (RH) is to provide an adsorbed layer of water on the surface which acts as a medium for the absorption and decomposition of atmospheric gases and for the dissolution of solid Ag into Ag^+ ions. The presence of an oxidising agent (e.g. O_3, NO_2) enhances the formation of Ag_2S by promoting the dissolution of bulk Ag (Graedel 1992). Similarly, enhanced corrosion rates have been observed in the presence of aerial oxygen, when compared to a pure N_2 environment (Kleber et al. 2008). The corrosion products formed in various outdoor environments have been found to be more complex than indoor environments and may include Ag_2O, AgO, AgCl and Ag_2SO_4 in addition to Ag_2S (Lin et al. 2013; Sanders et al. 2015).

The first direct measurements of the corrosion product of AgNPs when exposed to air identified secondary Ag_2S particles on the surfaces of the AgNPs and changes in the optical

✉ Vicki J. Keast
vicki.keast@newcastle.edu.au

[1] School of Information and Physical Sciences, University of Newcastle, Callaghan, NSW 2308, Australia

response of the particles in response to light (Elechiguerra et al. 2005; McMahon et al. 2005). There have been other subsequent studies identifying the corrosion product of AgNPs on exposure to ambient air as being Ag_2S (Cao and Elsayed-Ali 2009; Wang et al. 2011; Keast et al. 2016; Scuderi et al. 2016). That Ag predominantly corrodes to a sulfide is distinct from most other metals where the corrosion products on exposure to ambient air are usually oxides. In a number of the studies of corrosion of AgNPs, an a priori assumption was made that the corrosion product was an oxide and the possibility of Ag_2S as an explanation for the observed results do not appear to have been considered (Cai et al. 1998; Qi et al. 2010; Kuzma et al. 2012; Grillet et al. 2013). However, oxidation of AgNPs can be promoted using ozone concentrations greater than normal atmospheric levels (Qi et al. 2010; Han et al. 2011).

In contrast to other studies, an X-ray photoelectron spectroscopy (XPS) analysis of a 5 nm Ag film after exposure to laboratory air found predominantly only O on the surface, not S, with the exception of a film intentionally exposed to a high S environment (Oates et al. 2013). However, the RH of the laboratory environment was not reported, and a low RH can suppress Ag corrosion. Furthermore, XPS only reports the composition and valence of the top few atomic layers and the observations may represent adsorbed oxygen containing species on the surface, or the monolayer of AgO that is proposed to be associated with the dissolution of Ag in aqueous environments (Johnston et al. 2019). A similar XPS study on a Ag film observed the present of O, rather than S (Wang et al. 2017) but then assumed the observed corrosion product of AgNPs was an oxide without performing a direct verification. As the corrosion of AgNPs to Ag_2S is strongly enhanced when compared to bulk, this assumption may not be warranted. However, it cannot be excluded that in these two studies an unusually low concentration of H_2S and OCS in the ambient air inhibited the formation of Ag_2S.

Three possible routes, as illustrated in Fig. 1, have been identified for the conversion of AgNPs to Ag_2S in ambient air (Glover et al. 2011; Liu et al. 2011; Keast et al. 2016):

(1) direct conversion to Ag_2S;

(2) oxidative dissolution of Ag to Ag^+ followed by precipitation as Ag_2S; and

(3) oxidative dissolution of Ag to Ag^+ followed by precipitation as nanoparticulate Ag, then followed by conversion to Ag_2S.

Which of these processes dominate is likely to be determined by factors in the local environment such as: the RH (resulting in an adsorbed water layer); the presence of oxidative species; the concentration of sulfur containing gases such as H_2S and OCS; and exposure to light. The role of light may be to promote the photo-reduction of the Ag^+ species, present in the adsorbed water layer, to secondary Ag nanoparticles (Yu et al. 2014).

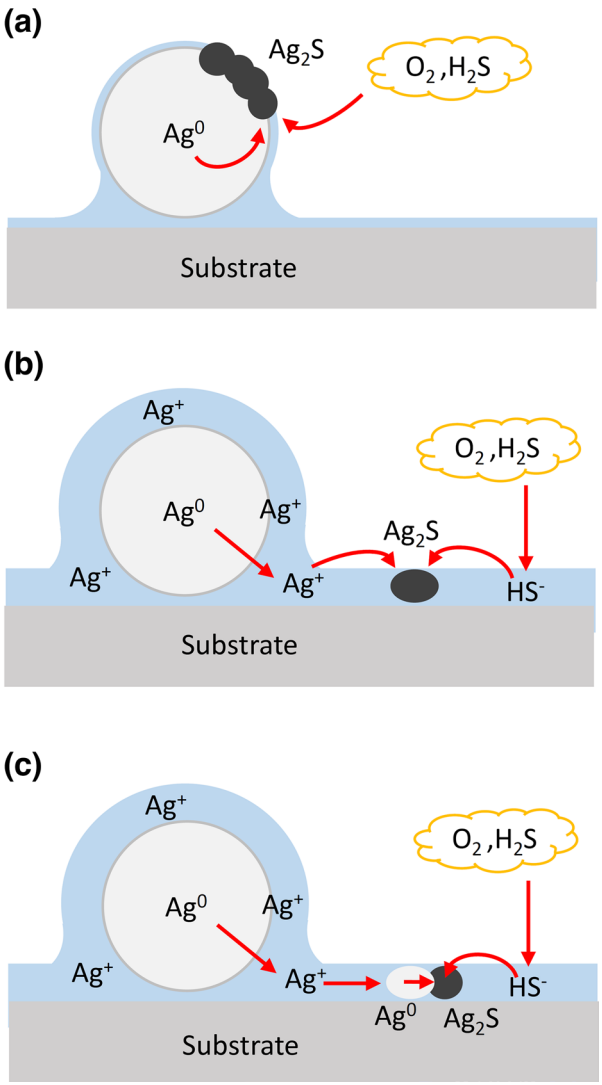

Fig. 1 Schematic of different possible corrosion processes for AgNPs. **a** Direct conversion to Ag_2S, **b** dissolution of Ag to Ag^+ followed by precipitation as Ag_2S. **c** dissolution of Ag to Ag^+ followed by precipitation as nanoparticulate Ag then conversion to Ag_2S

Although most evidence in the literature points to the corrosion product on the exposure of AgNPs to ambient air as being Ag_2S, there is sufficient ambiguity that development of additional methods to unequivocally identify Ag corrosion products is warranted. Electron energy loss spectroscopy (EELS) in the scanning transmission electron microscope (STEM) is a characterisation technique that can investigate the composition of nanostructured materials. In particular, the valence part of the spectrum ($< \sim 50$ eV) has a high interaction cross-section allowing high-quality spectra to be acquired relatively quickly. However, the shape of the valence EEL spectrum depends on the dielectric function of the material being studied and is thus an indirect measure of composition.

Despite considerable investigation into the corrosion of AgNPs, a consistent picture of their corrosion processes has not yet emerged. The role of environmental aspects, such as relative humidity (RH), the details of the atmospheric composition and exposure to light require further investigation. Further understanding of the corrosion behaviour would be advantageous to design approaches to address the rapid corrosion of AgNPs and to expand their range of applications. The aim of this work was to use electron microscopy imaging and analysis to investigate the early stages of AgNP corrosion under different conditions. Valence EELS has not previously been applied to the study of corrosion products in nanoparticle systems, and offers advantages in collection efficiency. This article will also report on the suitability of valence EELS to identify the corrosion products of Ag.

Methods

The AgNPs studied in this work were commercially available particles (Sigma-Aldrich catalogue number 758329) with a range of particle sizes under 100 nm in size, capped with polyvinylpyrrolidone (PVP) and dispersed in ethylene glycol at 5 wt.%. Samples for imaging and analysis in the STEM were further diluted in ethanol and deposited on a lacy carbon film supported on a copper grid. Each grid was then placed on filter paper in a small plastic petri storage container with a loose-fitting lid. The samples were stored in indoor environments for time periods varying from 24 h to 29 days. To investigate the role of RH, a set of samples were placed in secondary, non-airtight containers, with either an open container of water (to increase the RH), with silica desiccant (to decrease the RH) or alone. The effect of exposure to light was investigated by wrapping the petri storage container in Al foil.

STEM analysis was performed using a probe-corrected JEOL-ARM 200F STEM, operated at 200 kV with a probe size of ~ 0.1 nm. Bright field (BF) and annular dark field (ADF) images were acquired at a range of magnifications. Compositional analysis using X-ray energy dispersive spectroscopy (EDS) was performed using a JEOL Centurio SDD detector with 100 mm^2 detection area. EDS spectrum images were acquired using rapid raster acquisition with a cumulative dwell time per pixel of ~ 5 ms. Spectra from selected regions of the area mapped were extracted during post-processing. Acquisition and processing were performed using Thermo-Scientific NSS Software Version 4.0.

EELS was performed with a Gatan GIF Quantum spectrometer. The energy resolution for the EELS measurements was improved to around 0.5 eV by decreasing the extraction voltage on the cold field emission gun, giving a beam current of ~ 15 pA. EEL spectrum images were acquired with an energy dispersion of 0.05 eV per channel. Acquisition times at each pixel were typically around 0.1–0.2 s. After acquisition, Gatan's dark-current correction and energy drift correction routines were applied. The convergence and collection angles of the beam were ~ 24.9 mrad and ~ 8.8 mrad respectively. To map out the different components in the valence EELS spectrum, a multiple linear least squares fit (MLLS) to internal reference spectra of Ag, Ag_2S and C was made. This was followed by Gaussian peak fitting to the peaks in residual spectrum that corresponded to the surface plasmon peaks. Mapping composition with EELS using the S and Ag M ionisation edges was found to not offer any benefits over EDS due to the more complex processing required to extract elemental information, the presence of the C support film increasing the background signal, and the deleterious effects of C contamination on signal to background in EEL spectra. Plasma cleaning has been found to alter AgNPs and so cannot be used to reduce contamination rates in these experiments.

Valence EEL reference spectra were acquired from a range of materials representing possible corrosion products (AgO, Ag_2O, Ag_2S, Ag_2SO_4 and Ag_2CO_3) to facilitate identification of the corrosion product. These experimental spectra were compared to simulations using density functional theory (DFT) and in the random phase approximation (RPA) as implemented in the WIEN2k code (Blaha et al. 2001) and methods described previously (Keast 2013).

Results

Figure 2a–c shows images of AgNPs freshly deposited onto the lacey carbon film demonstrating that, as-deposited, they are free of any secondary particles attached to or in the vicinity of the otherwise pristine particles. Figure 2d–f shows representative images of particles after 24 h exposure to ambient air and Fig. 2g–i after 4 days exposure. Within 24 h secondary particles have appeared, and in general, these are larger after 4 days exposure although particles with a range of sizes have been observed for all exposure times. Contrary to expectation, no notable differences were observed between particles kept in the dark and those exposed to light. Many, but not all, of the secondary particles display a distinctive two-phase appearance of which examples are shown at higher magnifications in Fig. 2. The observed morphologies are consistent with previous work (Keast et al. 2016) where similar bimodal particles were associated with corrosion of triangular AgNPs. These were previously identified as having Ag and Ag_2S components, on the basis of the lattice images, and here that identification has been supported using EDS as shown in Fig. 3. As expected, the brighter regions in the ADF image are associated with predominantly Ag and the darker regions with a higher S content.

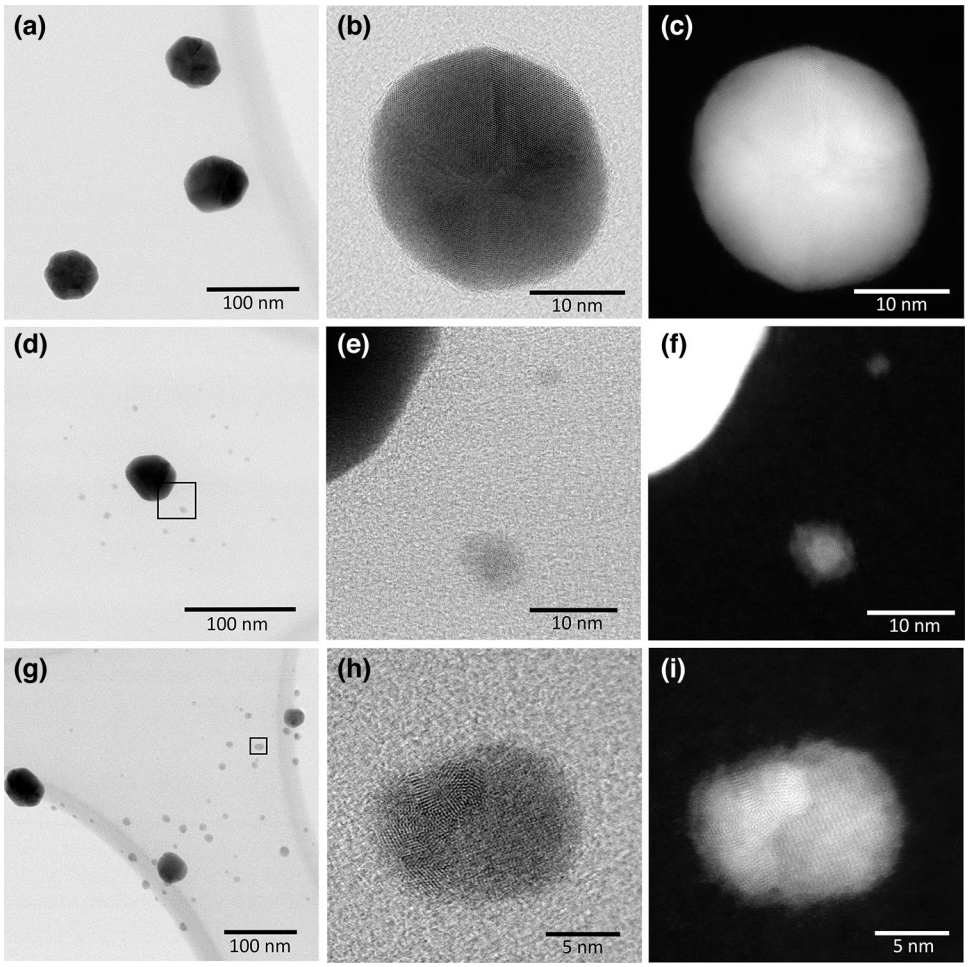

Fig. 2 **a**, **b** BF and **c** ADF images of as deposited AgNPs. **d**, **e** BF and **f** ADF images after 24 h of exposure to ambient air. **g**, **h** BF and **i** ADF images after 4 days of exposure to ambient air. The particles shown in **e,f** are those indicated by the box in (**d**) and the particle shown in **h**, **i** is the particle indicated by the box in (**g**)

Figure 4 shows the comparison between particles exposed to ambient air for 4 days (Fig. 4a) and 22 days (Fig. 4b) to that of particles stored in a low humidity environment with silica desiccant for 4 days (Fig. 4c) and 22 days (Fig. 4d). Fewer secondary particles are formed at low RH and those that do are attached to or close to the AgNPs. After 22 days in low RH the corrosion product, while still particulate in nature, has formed a shell around the original AgNPs, as opposed to the more dispersed distribution for exposure in ambient air. When exposed to the high RH environment a large number of secondary particles are formed over the entire support film and these secondary particles are composed of Ag and S, as shown in Fig. 5.

The small size of the secondary particles meant that valence EELS spectra were dominated by the substrate spectrum and it was not possible to reliably extract spectra representative of the particles alone. This was not improved when using Si_3N_4 membranes as a support film instead of lacey C. Therefore, EEL analysis was instead performed on particles with longer exposure times where a substantial amount of corrosion product had formed. Figure 6 shows results obtained from an AgNP exposed to ambient air for 29 days where the particle is suspended over a hole in the C support film. Three phases are observed: the AgNP; the corrosion product; and the C support film. In addition, surface plasmon peaks are observed with a higher energy plasmon peak at 2.8 eV, associated with the AgNP free of corrosion product, and a lower energy plasmon, at 2.1 eV, found at the edges of the corrosion product. This shift in the plasmon peak with corrosion is consistent with the observed plasmonic behaviour of AgNPs on exposure to air (McMahon et al. 2005). The reference spectra shown in Fig. 7 confirm that Ag_2S is the most probable candidate for the corrosion product, as expected based on the compositional data.

Discussion

The results presented here confirm that the corrosion product of AgNPs on exposure to ambient air is Ag_2S and that the corrosion process is mediated by the generation of secondary particles. The RH plays an important role with the number and spread of the secondary particles increasing with RH. The results demonstrate that the role of RH in

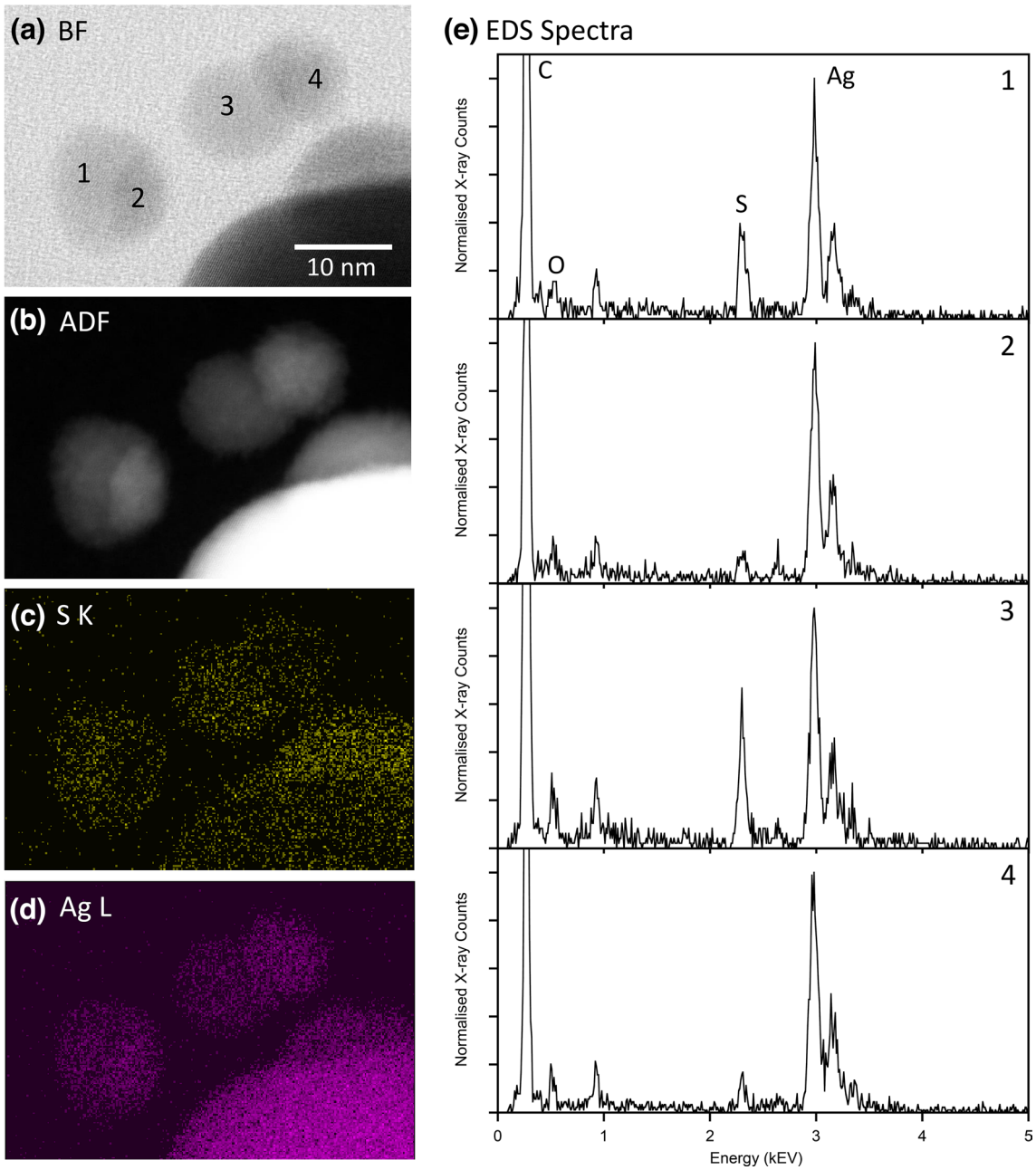

Fig. 3 **a** BF and **b** ADF images of AgNP particles after 4 days exposure to laboratory air. Corresponding EDS maps of **c** S K counts and **d** Ag L counts. **e** EDS spectra extracted from the regions indicated in **a**. Spectra have been rescaled to the Ag L peak

the corrosion process is to allow dispersion of Ag^+ ions through the adsorbed water layer, providing a larger number of secondary particles which will accelerate corrosion rates. The observations reported here are consistent with the formation of secondary particles on bulk Ag (Glover et al. 2011) and the role of RH. In contrast, no difference was observed between AgNPs kept in the dark and those exposed to light. However, it is possible that the nucleation of the small nanoparticles occurred during sample preparation during the evaporation of the solution after deposition on the carbon film.

A limitation of this study is that the effect of environmental variables was only studied qualitatively. Future experiments with more careful quantitative control of RH and H_2S levels are desirable. Whilst RH can be controlled experimentally relatively readily, the typical concentration of H_2S in the atmosphere are in the parts per billion (ppb) range (Pope et al. 1968; Rice et al. 1981; Chou 2003) and

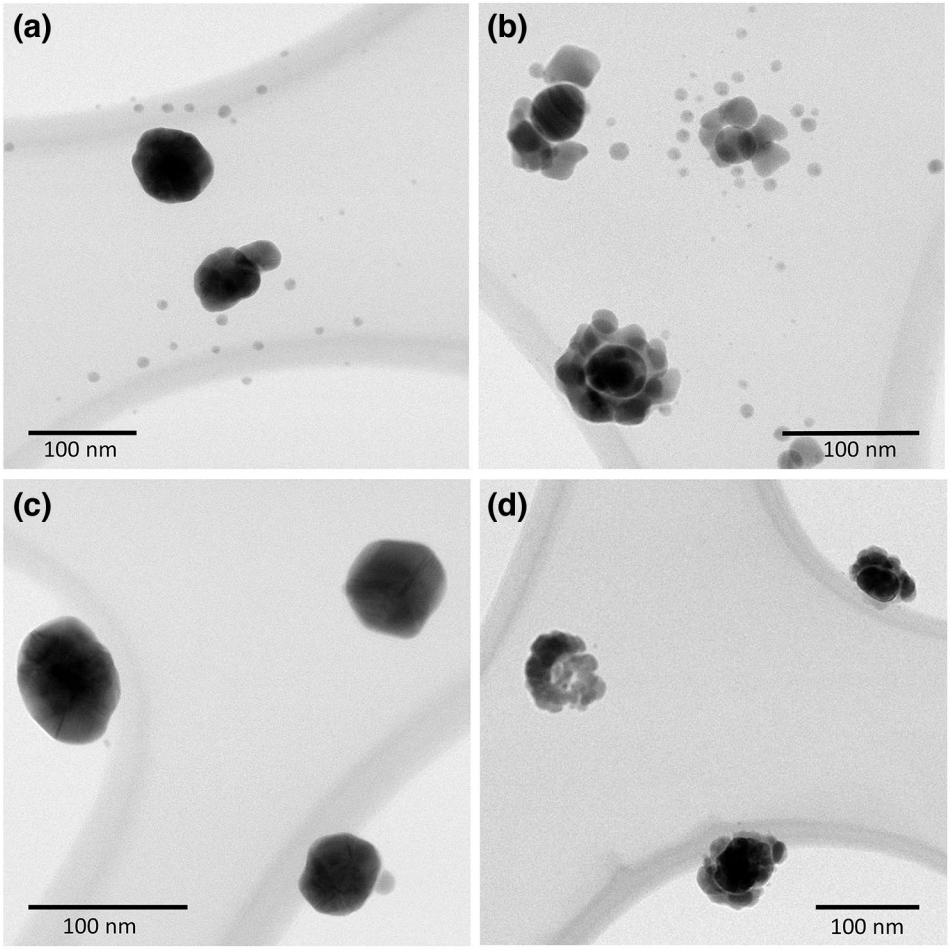

Fig. 4 BF STEM images of AgNPs exposed to ambient air for **a** 4 days and **b** 22 days. BF STEM images of AgNPs stored in a low humidity environment with silica desiccant for **c** 4 days and **d** 22 days

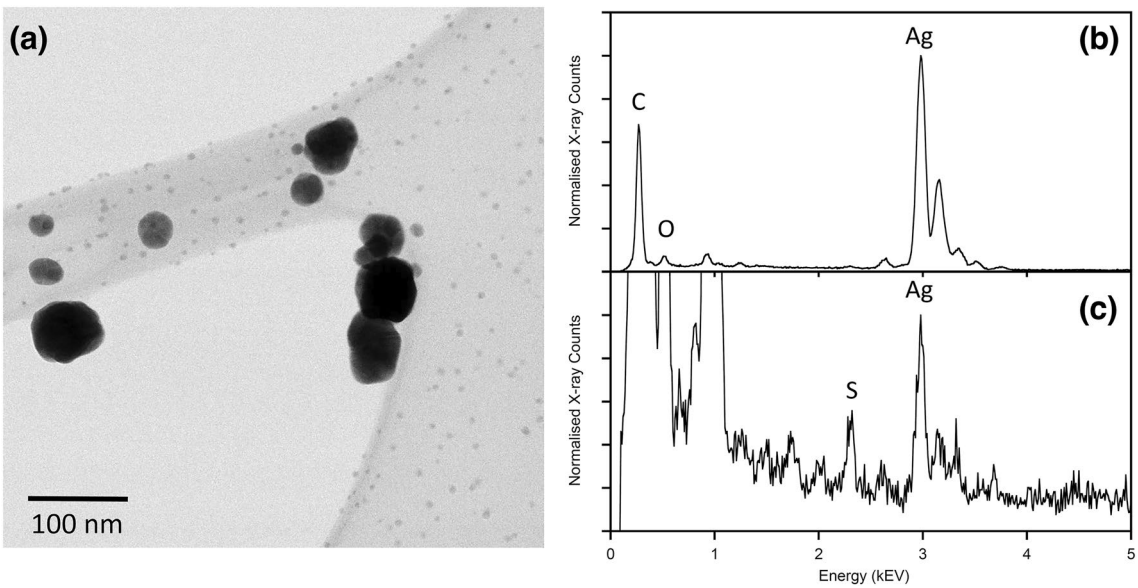

Fig. 5 **a** BF STEM images of AgNP particles after 4 days exposure to a high RH environment. **b** EDS spectra extracted from an AgNP and **c** EDS spectra from a region of the support film and secondary particles. Spectra have been rescaled to the Ag L peak

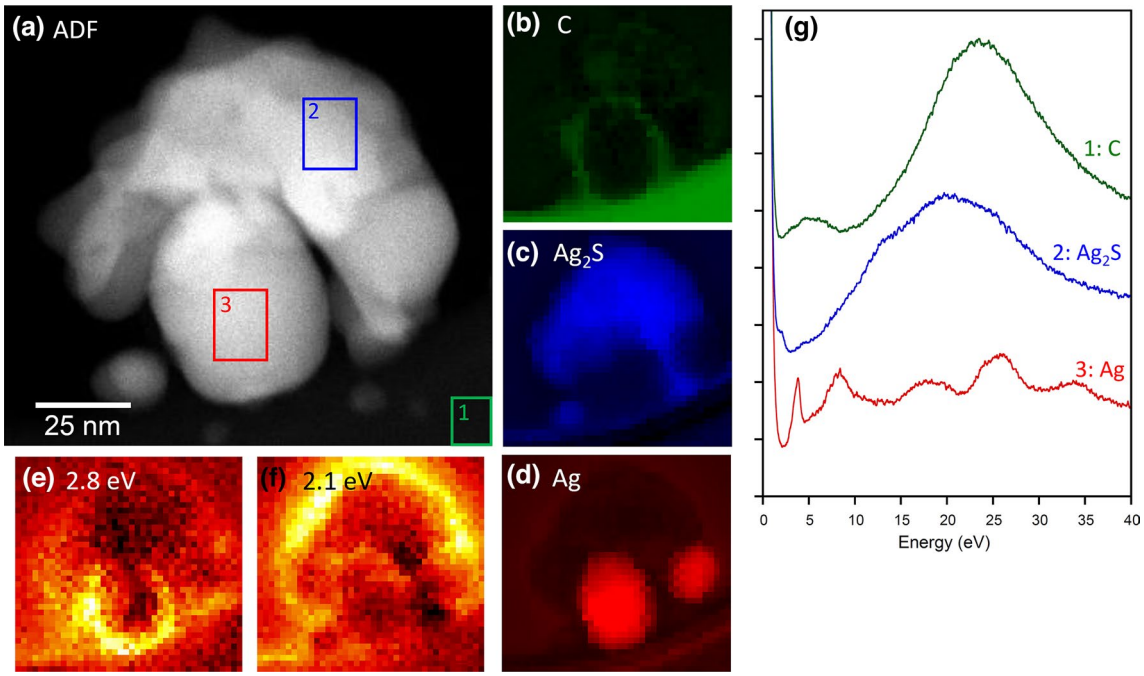

Fig. 6 a ADF image of AgNP particle after 29 days exposure to ambient air. **b–d** EELS phase maps generated using internal reference spectra. **e**, **f** Maps of surface plasmon peaks. **g** Internal reference spectra extracted from the regions indicated in **a** and used to generated the phase maps

these are very challenging to both measure and control. For this reason, many prior experiments of Ag corrosion were conducted with much higher H_2S concentrations. However, the corrosion processes in these accelerated environments may not reflect those in typical environmental conditions.

The DFT calculations of the valence EELS show general agreement with the overall experimental spectral shapes. The zero-loss-peak has not been extracted from the experimental spectra accounting for the difference at low energies. Some peaks at high energies are more intense in the calculated spectra due to the influence of local field effects (Vast et al. 2002). More sophisticated approaches can be used to address local field effects as well as many-body interactions, but these are significantly more computationally demanding (Onida et al. 2002). The DFT results presented here are sufficient to confirm that the experimental spectra correspond to what is expected for these reference compounds.

These results demonstrate that valence EELS can be used to identify the spectral signature of the corrosion product and this can be mapped at the nanometre scale. However, interference from the substrate and the plasmonic response of AgNPs make this challenging for very small particles. Ultrathin carbon or graphene substrates are recommended for the study of smaller particles. By comparison with reference spectra, the corrosion product can be unambiguously identified as Ag_2S and so using this approach may be useful for wider studies of corrosion products both in the nanoparticle and bulk forms. Such an approach may be useful for the study of copper corrosion in outdoor environments where many different corrosion products may form (Graedel 1987). In addition, this is the first direct observation at the nanoscale on the alteration to the surface plasmon as a consequence of the formation of a corrosion product. It has been well established from optical spectra that the effect of corrosion is the dampen and shift the energy of the plasmon resonance, but the spatially resolved nature of the EELS measurements presented here demonstrate that the plasmon resonance occurs at the edge of the corrosion product, not at the interface between the AgNP and the corrosion product.

Conclusions

We have examined the role of environmental variables on the corrosion of AgNPs and found RH plays an important role on the number and distribution of corrosion products. On exposure to ambient air AgNPs produce secondary particles and these particles corrode to Ag_2S. In low RH the particles are clustered around and attached to the parent nanoparticles but higher RH allows released Ag^+ ions to migrate across the substrate and secondary particles can be found at significant distances away. Storing AgNPs at low RH can be expected to extend their life. Valence EELS offers a useful approach to identify the corrosion product and can also reveal the impact of the corrosion product on the surface plasmon properties. Although extracting

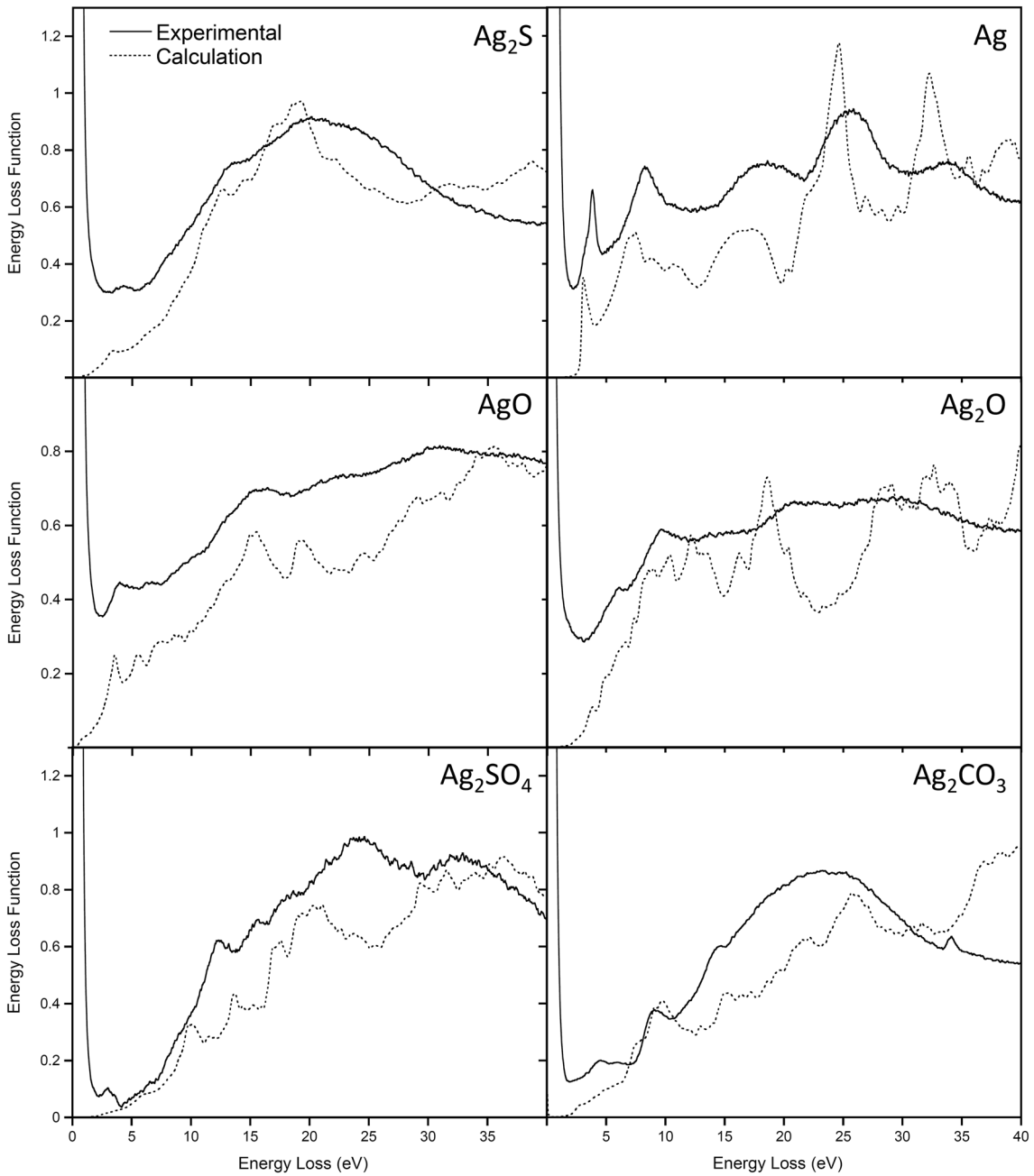

Fig. 7 Experimental valence EEL spectra from reference compounds compared to computed spectra using DFT and the RPA

the different components contributing to the valence EEL spectrum can be challenging, the technique offers the opportunity to acquire various types of information within a single spectrum image.

Acknowledgements The author acknowledges use of facilities within the University of Wollongong Electron Microscopy Centre.

Funding Open Access funding enabled and organized by CAUL and its Member Institutions.

Declarations

Conflict of interest The author states that there is no conflict of interest.

References

Alexander JW (2009) History of the medical use of silver. Surg Infect 10:289–292

Barillo DJ, Marx DE (2014) Silver in medicine: a brief history BC335 to present. Burns 40S:S3–S8

Bennett HE, Peck RL, Burge DK, Bennett JM (1969) Formation and growth of tarnish on evaporated silver films. J Appl Phys 40:3351–3360

Blaha P, Schwarz K, Madsen GKH, Kvasnicka D, Luitz J (2001) WIEN2K, n augmented plane wave plus local orbitals program for calculating crystal properties. Technische Universitat Wien, Austria

Cai W, Zhong H, Zhang L (1998) Optical measurements of oxidation behavior of silver nanometer particle within pores of silica host. J Appl Phys 83:1705–1710

Cao W, Elsayed-Ali HE (2009) Stability of Ag nanoparticles fabricated by electron beam lithography. Mater Lett 63:2263–2266

Chou CH (2003) Hydrogen Sulfide: human health aspects. Concise International Chemical Assessment Document 53. World Health Organisation, Geneva

Elechiguerra JL, Larios-Lopez L, Lui C, Garcia-Gutierrez D, Camacho-Bragado A, Yacaman MJ (2005) Corrosion at the nanoscale: the case of silver nanowires and nanoparticles. Chem Mater 17:6042–6052

Franey JP, Kammlott GW, Graedel TE (1985) The corrosion of silver by atmospheric sulfur gases. Corros Sci 25:133–143

Glover RD, Miller JM, Hutchinson JE (2011) Generation of metal nanoparticles from silver and copper objects: nanoparticle dynamics on surfaces and potential sources of nanoparticles in the environment. ACS Nano 5:8950–8957

Gorham JM, Rohlfing AB, Lippa KA, MacCuspie RI, Hemmati A, Holbrook RD (2014) Storage wars: how citrate capped silver nanoparticle suspensions are affected by not-so-trivial decisions. J Nanopart Res 16:2339

Graedel TE (1987) Copper patinas formed in the atmosphere - II. A qualitative assessment of mechanisms. Corros Sci 27:721–740

Graedel TE (1992) Corrosion mechanisms for silver exposed to the atmosphere. J Electrochem Soc 139:1963–1970

Graedel TE, Franey JP, Gualtieri GJ, Kammlott GW, Malm DL (1985) On the mechanism of silver and copper sulfidation by atmospheric H2S and OCS. Corros Sci 25:1163–1180

Grillet N, Manchon D, Cottancin E, Bertorelle F, Bonnet C, Broyer M, Lerme J, Pellarin M (2013) Photo-oxidation of individual silver nanoparticles: a real-time tracking of optical and morphological changes. J Phys Chem C 117:2274–2282

Han Y, Lupitsky R, Chou TM, Stafford CM, Du H, Sukhishvila S (2011) Effect of oxidation on surface-enhanced Raman scattering activity of silver nanoparticles: a quantitative correlation. Anal Chem 83:5873–5880

Johnston KA, Stabryla LM, Gilbertson LM, Millstone JE (2019) Emerging investigator series: connecting concepts of coinage metal stability across length scales. Environ Sci Nano 6:2674–2696

Keast VJ (2013) An introduction to the calculation of valence EELS: Quantum mechanical methods for bulk solids. Micron 44:93–100

Keast VJ, Myles TA, Shahcheraghi N, Cortie MB (2016) Corrosion processes of triangular silver nanoparticles compared to bulk silver. J Nanopart Res 18:45

Kleber C, Wiesinger R, Schnöller J, Hilfrich U, Hutter H, Schreiner M (2008) Initial oxidation of silver surfaces by S^{2-} and S^{4+} species. Corros Sci 50:1112–1121

Kuzma A, Weis M, Flickyngerova S, Jakabovic J, Satka A, Dobrocka E, Chlpik J, Cirak J, Donoval M, Telek P, Uherek F, Donoval D (2012) Influence of surface oxidation on plasmon resonance in monolayer of gold and silver nanoparticles. J Appl Phys 112:130531

Le Ouay B, Sellacci F (2015) Antibacterial activity of silver nanoparticles: a surface science insight. Nano Today 10:339–354

Lin H, Frankel GS, Abbott WH (2013) Analysis of Ag corrosion products. J Electrochem Soc 160:C345–C355

Liu J, Pennell KG, Hurt RH (2011) Kinetics and mechanisms of nanosilver oxysulfidation. Environ Sci Technol 45:7345–7353

McMahon MD, Lopez R, Meyer HM, Feldmen LC, Haglund Jr RF (2005) Rapid tarnishing of silver nanoparticles in ambient laboratory air. Appl Phys B 80:915–921

Oates TWH, Lusardo M, Noda S, Hinrichs K (2013) The effect of atmospheric tarnishing on the optical and structural properties of silver nanoparticles. J Phys D Appl Phys 46:145308

Onida G, Reining L, Rubio A (2002) Electronic excitations: density-functional versus many-body Green's-function approaches. Rev Mod Phys 74:601–659

Pastoriza-Santos I, Liz-Marzan LM (2008) Colloidal silver nanoplates. State of the art and future challenges. J Mater Chem 18:1724–1737

Pope D, Gibbens HR, Moss RL (1968) The tarnishing of Ag at naturally-occurring H_2S and SO_2 levels. Corros Sci 8:883–887

Qi H, Alexson D, Glembocki O, Prokes SM (2010) The effect of size and size distribution on the oxidation kinetics and plasmonics of nanoscale Ag particles. Nanotechnology 21:215706

Rice DW, Peterson P, Rigby EB, Phipps PBP, Coppell RJ, Tremoureux R (1981) Atmospheric corrosion of copper and silver. J Electrochem Soc 128:275–284

Rizzello L, Pompa PP (2014) Nanosilver-based antibacterial drugs and devices: Mechanisms, methodological drawbacks, and guidelines. Chem Soc Rev 43:1501–1518

Rycenga M, Cobley CM, Zeng J, Li W, Moran CH, Zhang Q, Qin D, Xia Y (2011) Controlling the synthesis and assembly of silver nanostructures for plasmonic applications. Chem Rev 111:3699–3712

Sanders CE, Verreault D, Frankel GS, Allen HC (2015) The role of sulfur in the atmospheric corrosion of silver. J Electrochem Soc 162:C630–C637

Scuderi M, Esposito M, Todisco F, Simeone D, Tatamtini I, De Marco L, De Giorgi M, Nicotra G, Carbone L, Sanvitto D, Passaseo A, Gigli G, Cuscunà M (2016) Nanoscale study of the tarnishing process in electron beam lithography-fabricated silver nanoparticles for plasmonic applications. J Phys Chem C 120:24314–24323

Vast N, Reining L, Olevano V, Schattschneider P, Jouffrey B (2002) Local field effects in the electron energy loss spectra of rutile TiO2. Phys Rev Lett 88:037601

Wang L, Xiong W, Nishijima Y, Yokota Y, Ueno K, Misawa H, Bi G, Qiu JR (2011) Spectral properties and mechanism of instability of nanoengineered silver blocks. Opt Express 19:10640–10646

Wang X, Santschi C, Martin OJF (2017) Strong improvement of long-term chemical and thermal stability of plasmonic silver nanoantennas and films. Small 13:1700044

Yu S, Yin Y, Chao J, Shen M, Liu J (2014) Highly dynamic PVP-coated silver nanoparticles in aquatic environments: chemical and morphology change induced by oxidation of Ag^0 and reduction of Ag+. Environ Sci Technol 48:403–411